Dalton Transactions

ROYAL SOCIETY OF CHEMISTRY

PAPER

View Article Online
View Journal | View Issue

Cite this: *Dalton Trans.*, 2025, **54**, 3013

Understanding non-reducible N_2 in the mechanism of Mo–nitrogenase†

Ian Dance

In my proposed mechanism of Mo–nitrogenase there are two roles for separate N_2 molecules. One N_2 diffuses into the reaction zone between Fe2 and Fe6 where a strategic gallery of H atoms can capture N_2 to form the Fe-bound HNNH intermediate which is then progressively hydrogenated through intermediates containing $HNNH_2$, NH and NH_2 entities and then two NH_3 in sequence. The second N_2 can be parked in an N_2-pocket about 3.2 Å from Fe2 or bind end-on at the *exo* coordination site of Fe2. This second N_2 is outside the reaction zone, not exposed to H atom donors, and so is 'non-reducible'. Here density functional calculations using a 485+ atom model describe the thermodynamics for non-reducible N_2 moving between the N_2-pocket and the *exo*-Fe2 position, for the resting state and 19 intermediates in the mechanism. The entropy component is estimated and included. The result is that for all intermediates with ligation by H or NH_x at the *endo*-Fe2 position the free energy for association of non-reducible N_2 at *exo*-Fe2 is negative. There remains some uncertainty about the status of *exo*-Fe2–N_2 during the step in which H_2 exchanges with the incoming reducible N_2, where at least two unbound molecules are present. At Fe2 it is evident that attainment of octahedral coordination stereochemistry dominates the binding thermodynamics for non-reducible N_2. Possibilities for experimental support of these computational conclusions are discussed.

Received 11th November 2024,
Accepted 3rd January 2025

DOI: 10.1039/d4dt03146f

rsc.li/dalton

1. Introduction

Nitrogenase, the enzyme that has evolved as the natural source of nitrogen for the earth's biosphere,[1] catalyses the conversion of inert N_2 to NH_3 under ambient conditions which contrast strongly with the extreme conditions required for the Haber–Bosch industrial manufacture of ammonia.[2] How does the enzyme achieve a catalysis that chemists have failed to replicate?[3,4] Extensive experimental investigation involving reaction kinetics,[5,6] mutations of amino acids surrounding the active site,[7–21] vibrational and spin resonance spectroscopy,[22–30] crystal structures,[31,32] cryo-electron microscopy[4,33] and density functional simulations.[34–43] still leave many aspects of the chemical mechanism unresolved.

This is partly due to experimental difficulties in isolating and investigating intermediates under physiological turnover conditions, because unavoidable protons are a substrate of the enzyme and mixtures of transient intermediates occur.[32,44] Furthermore, the overall chemical reaction eqn (1) implies a mechanistic cycle with at least 27 steps: eight introductions of a proton, eight additions of an electron, N_2 binding, breaking the N–N bond, formation of six N–H bonds, two dissociations of NH_3 and formation of one H–H bond.

$$N_2 + 8e^- + 8H^+ \rightarrow 2NH_3 + H_2 \quad (1)$$

The protein domain in which this chemistry occurs is shown in Fig. 1. The catalytically active site is the iron–molybdenum cofactor, FeMo-co, a CFe_7MoS_9 cluster with homocitrate and His442 coordination to Mo and Cys275 coordination at Fe1: throughout this paper amino acids are numbered according to crystal structure PDB 3U7Q of Mo–nitrogenase species *Azotobacter vinelandii* (*Av*). Mutagen-reactivity experiments show that the active domain of FeMo-co is the front face, Fe2–S2B–Fe6–S3B–Fe7 enclosed by Val70 and Arg96.[8,10–12,17,19,45–49] There is a significant hydrogen bond between Nε of His195 and S2B. The four penultimate water molecules of the proton supply chain are shown, with hydrogen bonds to O3, O6 and O5 of homocitrate, and the final proton directed towards S3B. Protons are translocated along the complete chain (not shown) by a Grotthuss mechanism.[50]

Fig. 1 also marks the vicinity of the N_2-pocket. This is a position where N_2 can be parked ready to bind at *exo*-Fe2. As shown in Fig. 2 this pocket lies on a hydrophobic N_2 ingress channel intruding from the protein surface towards Fe2. Smith *et al.* explored this pathway with molecular dynamics simulations,[51] and showed how it is gated at the protein surface by significant

School of Chemistry, UNSW Sydney, NSW 2052, Australia.
E-mail: i.dance@unsw.edu.au

† Electronic supplementary information (ESI) available. See DOI: https://doi.org/10.1039/d4dt03146f

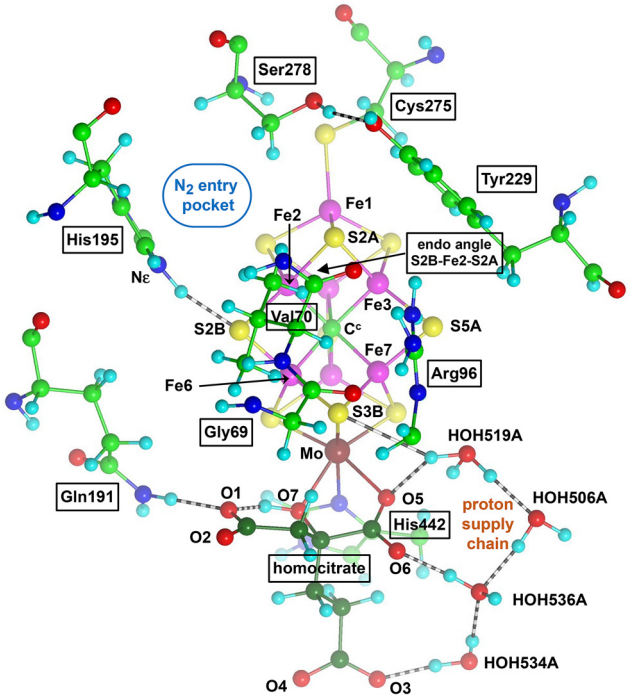

Fig. 1 Structure of the active site of Mo–nitrogenase, with FeMo-co at the centre. Significant surrounding amino acids (all in the α-domain) and water molecules are included, with labels for *Av*1 protein, crystal PDB 3U7Q. Homocitrate C atoms are dark green and hydrogen bonds are striped. The reaction zone is the Fe2–Fe6–Fe7 face, under the side chain of Val70 and bounded by the side chain of Arg96. The proposed N_2 entry pocket is between His195 and Ser278, approaching Fe2. The four penultimate water molecules of the proton supply chain are shown, with hydrogen bonds to O3, O6 and O5 of homocitrate, and with the final proton directed towards S3B.

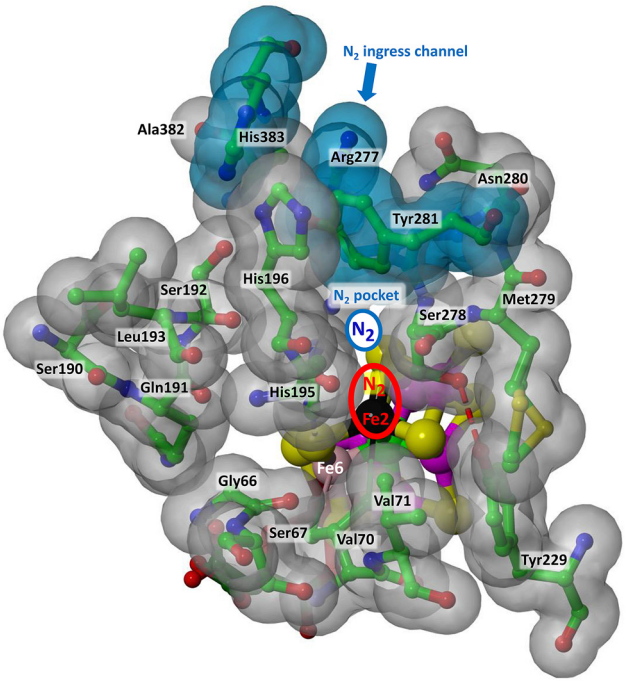

Fig. 2 The putative N_2 ingress channel and N_2-pocket (blue enclosure) in structure PDB 3U7Q. The blue shaded residues, His383, Arg281 and Tyr277 are at the surface opening of the channel.[51] Exogenous N_2 can enter this hydrophobic channel and park in the N_2-pocket located between the His196–His195 chain on one side and Ser278 on the other, and then move from the N_2-pocket to the *exo* coordination position of Fe2, indicated by the red enclosure.

movements of residues His383, Tyr281 and Arg277, shaded blue on Fig. 2. The free energy change for passage of exogenous N_2 through this ingress channel was calculated as *ca.* +3 kcal mol^{-1}.[51] Gee *et al.* studied the pathway taken by CO photolabilised from *exo*-Fe2–CO, including a 'docking site' about 5 Å from Fe2. This docking site for CO is close to the N_2-pocket.

1.1. Overall mechanism

Using density functional simulations with a 485+ atom model of the active domain, I have developed a chemical mechanism for the complete cycle that effects eqn (1). The sequence of intermediates and reaction steps is outlined in Scheme 1. In Panel A the green enclosure describes the preparative phase, accumulating H atoms on FeMo-co, and the yellow enclosure shows the formation of bound H_2, the H_2/N_2 exchange, and the capture of N_2 to form the intermediate with bound HNNH. This crucial step in which N_2 is activated has been described in detail.[52] Panel B of Scheme 1 describes the subsequent steps in which the N–N bond is broken with concerted formation of NH_3 bound at Fe6, and subsequent dissociation of this first NH_3. Details of the reactions and intermediates in the Panel B part of the mechanism have also been published.[53] Panel C of Scheme 1 outlines the steps and intermediates involved in formation and dissociation of the second NH_3, and finally recovery of the resting state.

Other authors have proposed different mechanisms for all or parts of the Mo–nitrogenase reaction.[35,40,42,43,54–64] I have reviewed mechanisms proposed prior to 2020.[37] The reason for presenting my new full mechanism here will become evident in the following section, where the dual roles of N_2 in the mechanism are described, and the question investigated in the present paper is explained.

1.2. Dual roles of N_2

The N_2 entry pocket located between His195 and Ser278 is near the *exo* coordination position of Fe2, where end-on (η^1) coordination of N_2 is feasible.[66] The position of this *exo*-Fe2–N_2 entity is emphasised in red on Fig. 2. It is possible for a second N_2 molecule to enter along this ingress channel, then diffuse past *exo*-Fe2–N_2 and enter the reaction zone,[66,67] where, after exchanging with H_2 it is captured in the N_2 activation step[52] (yellow enclosure of Scheme 1 Panel A). It is also possible that N_2 can approach FeMo-co along a different path described by Morrison *et al.* following investigations of the protein structure with the CAVER software. This alternate path passes near the sidechains of Tyr229, Val70, Met279, Ser278 and Cys275 and is discussed further in section 4.2.

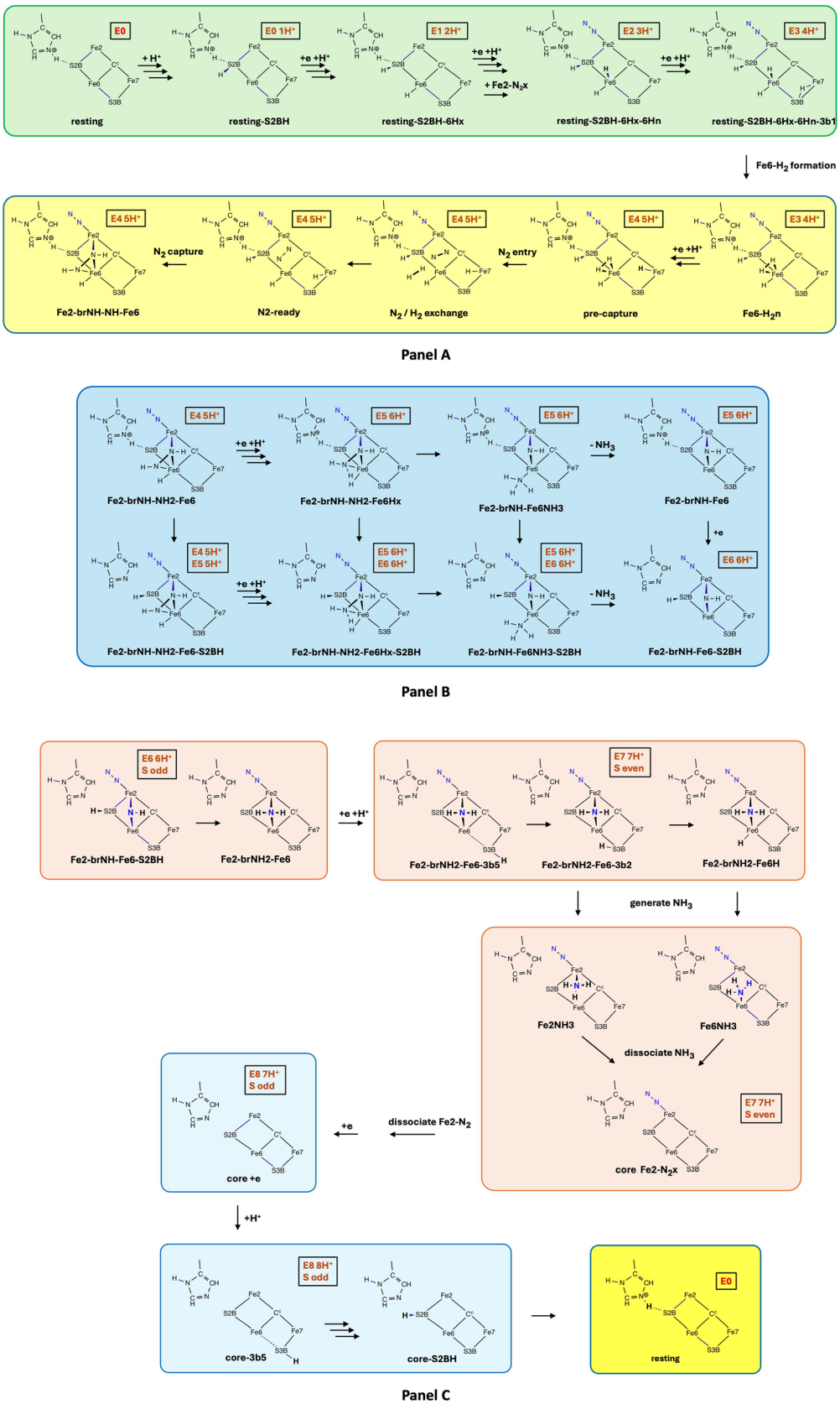

Scheme 1 The full cycle for my proposed chemical mechanism of nitrogenase, showing all major intermediates and reaction steps in minimal skeleton representation. At each stage the numbers of added electrons and protons are indicated by the red status boxes. The arrow clusters indicate the sequence of steps in which a proton is introduced from the proton supply chain[37,50] onto S3B, probably triggered by entry of an electron,[65] followed by reconfiguration of S3B–H and migration as H atoms across the cluster to sites on Fe atoms or to S2B.

At this point it is important to recognise that there is no experimental evidence for N_2 at the *exo*-Fe2 position in any of the multiple crystal structures of the resting protein. This raises a basic question, which is the subject of this paper. If *exo*-Fe2–N_2 is absent in the resting state, what is its participation in the many other intermediates and reaction steps? Reference to Scheme 1 shows *exo*-Fe2–N_2 marked as present in the central stages of the overall reaction. In this paper I report computational results on the thermodynamics of N_2 binding at *exo*-Fe2 and rationalise the occurrence of *exo*-Fe2–N_2 in the various intermediates of the cycle.

N_2 at *exo*-Fe2 is not entirely passive, because it can have a mechanistic role. The HD reaction of nitrogenase, $D_2 + 2e^- + 2H^+ \rightarrow 2HD$, occurs only in the presence of N_2.[68–70] There are many experimental data relating to the HD reaction: they are mechanistically informative and are summarised in ref. 71. A key datum is that the $K_m(N_2)$ for HD formation and the $K_m(N_2)$ for NH_3 production are different.[70] I have reported a computationally simulated detailed mechanism for the HD reaction, which accounts for all experimental data, and in which *exo*-Fe2–N_2 is the promoting N_2. To differentiate the two roles, N_2 that is reduced by nitrogenase to NH_3 was dubbed 'reducible' N_2, and N_2 that is not reduced but is required for the HD reaction was dubbed 'promotional' N_2.[67]

Promotional N_2 coordinated at the *exo*-Fe2 position is located away from potential hydrogen atom donors, and hydrogenation of this N_2 is not feasible. There is a clear differentiation of 'reducible' N_2 that enters a strategically propitious gallery of H atoms in the reaction zone between Fe2 and Fe6,[52] and *exo*-Fe2–N_2 which is awkwardly positioned for the formation of H–N bonds,[67] and is labeled 'non-reducible' N_2 in this paper.

The objective of the investigation reported below is to determine when non-reducible N_2 is present in the intermediates of Scheme 1. What are the thermodynamics and kinetics for movement of the N_2 molecule between a parked position in the N_2-pocket, or coordinated at *exo*-Fe2? This information is needed to justify correct models, with *exo*-Fe2–N_2 included or excluded, in calculations of the thermodynamics of each of the steps in the complete mechanism, Scheme 1.

2. Methodology

2.1. Model

The computed protein model is a 485+ atom extract from crystal PDB 3U7Q, including all relevant amino acids. This is my standard model for simulations of nitrogenase reactions and reactivity.[37,39,52,53,66,71] This model includes nine of the ten active-site residues that are conserved across all analyzed extant nitrogenases:[72] the exception Gly424 is outside the reaction zone. Details, and the rationale for inclusion of amino acids and truncation of uninvolved side chains, are provided in the ESI.† The coordinated alcoholate O7 atom of homocitrate is protonated and hydrogen bonded to O1. The standard constraining strategy with 28 distance constraints is described in the ESI.† At some stages in the mechanism the protein structure is expanded slightly in the reaction zone, as previously described and rationalised, and this is controlled *via* the distance constraints Cα(Val70)–C^c and Cα(Val70)–CZ(Arg96), here set to the values used in prior calculations of the intermediates and reaction steps.[52,53] At the H_2/N_2 exchange stage there are two unbound molecules, H_2 and reducible N_2, and therefore calculation of the *exo*-Fe2–N_2 binding trajectories required additional constraints for stability of the computational model: the coordinates of unbound H_2 and unbound reducible N_2 were fixed.

2.2. Electronic states

The electronic states of FeMo-co and its ligated forms are characterised by the spin densities on the Fe atoms, and the total spin S. There are multiple combinations of positive and negative spin densities on the Fe atoms, and I have previously presented a qualitative theory of relative stability, based on maximisation of antiferromagnetic interactions (opposite spin signs, weakly bonding) along the axial edges of the central Fe_6 prism of FeMo-co.[67] Intermediates with ligation at Fe2 and/or Fe6 usually have diminished Fe spin densities relative to Fe3, Fe4, Fe5, Fe7 and so the antiferromagnetic interactions involving Fe2 and Fe6 are less stabilising than the two other possibilities with oppositely signed spin pairs Fe3–Fe7 or Fe4–Fe5. These two favourable electronic states have negative spin densities on Fe3 and Fe5 (labelled '35'), or on Fe4 and Fe7 ('47'). Diagrams explaining this argument are provided in ref. 67. The superior stability of the '35' and '47' electronic states is consistent with the findings and procedures of other authors,[34,35,40–43,73–76] and these states were used in the present calculations, consistent with the spin and electronic states used for calculation of the reaction steps in the mechanism.

The DMol procedure for control of electronic states involves input of signs and starting magnitudes of atom spin densities, which are then able to adjust without constraint during scf convergence. This permits electronic states to change during an energy minimisation calculation, and all reaction trajectories were checked for such changes. Control of electronic states in the calculations reported here was *via* input spin populations for Fe1, Fe3, Fe4, Fe5 and Fe7.

2.3. DMol protocol

Density functional (DF) calculations use the DMol methodology of Delley,[77–82] using numerical DF solutions of free atoms for the basis sets. The basis set is DNP (double numerical plus polarisation). Details of this methodology and its advantages are contained in refs. 77 and 80. Highly accurate DFT solutions for the separated atoms limit are obtained. This methodology intrinsically provides reliable energies at long interatomic distances, and is capable of accurate descriptions of weak bonding and dispersion energies. The ability of the DMol methodology to incorporate long-range dispersion has been well demonstrated. Zhang *et al.* reported very good agreement between the experimental interatomic potential energy curves and the DMol/PBE calculated potential energy curves for the inert-gas pairs He_2 Ne_2 and HeNe, and excellent agreement for the HeAr and NeAr pairs relevant to the dispersion interactions in the nitrogenase inter-

mediates.[83] Todorova and Delley used this DMol/DNP/PBE methodology to optimize the crystal structures of a comprehensive set over 40 molecular crystals in which dispersion and intermolecular interactions determine the crystal packing and crystal lattice parameters.[82] This set of molecular crystals ranged over amino acids, aliphatic and aromatic hydrocarbons, ice, H_2S, S_8, C_{60}, and the inert gases Ne, Ar, Kr and Xe. The PBE functional overestimates lattice parameters by about 4%, while the PBE_{sol} functional yields lattice parameters with an average systematic error of less than 1%. The dispersion interactions in this variety of molecular crystals are very similar to those in proteins.

The calculations were all-electron, spin-unrestricted, with no imposed symmetry. The conductor-like screening model (COSMO)[84–86] was used with a dielectric constant of 5. Constraints on interatomic distances used the Lagrange Multiplier Algorithm. Output spin populations were calculated by the Mulliken method.[87]

2.4. Validation

Assessment of the accuracy of the computational procedures is made through reference to experimental geometrical and thermochemical data. Thorhallsson *et al*. consider that agreement with the dimensions of the crystal structure is essential for gauging the quality of the computational protocols.[35] Table 1 shows that the agreement between calculated and experimental lengths for C^c–Fe bonds and for Fe–S bonds in resting FeMo-co is 0.01 Å or better. Specific distances, tabulated in the ESI,† have an average deviation of 0.02 Å between calculated and experimental.

The DMol/PBE method reproduces experimental enthalpy data on the binding of N_2. Relevant $\Delta H_{exp}/\Delta H_{calc}$ comparisons from ref. 88 (kcal mol^{-1}) are: (a) exp 17.6, calc 20.0, 18.8; (b) exp ~10, calc 10.2; (c) exp 22.8, calc 25.9. Other relevant assessments of DMol accuracy *vs*. experiment have examined the electron affinities of atoms and molecules,[89] the enthalpies of formation for small (<100 electrons) molecular and atomic species,[90] the structures of metal–sulfide clusters,[91] photo-induced conversion of $[Os(NH_3)_5(\eta^1\text{-}N_2)]^{2+}$ to $[Os(NH_3)_5(\eta^2\text{-}N_2)]^{2+}$ (*i.e.* end-on to side-on bonding of N_2),[92] the geometry and vibrational frequencies of $[(NH_3)_5Ru(pyrazine)Ru(NH_3)_5]^{4+,5+,6+}$,[93] and protonation reactions involving hydrogen bonding.[94]

2.5. Mapping the potential energy surface

My calculations of the reactivity and reactions of nitrogenase, and the development of mechanism, are based on the mapping of potential energy surfaces. The revealed energy minima, as possible intermediates, are assessed by mapping the potential energy ridge(s) between them, and locating transition states. This deploys a general procedure,[37,50,95,96] that works well for multidimensional potential energy surfaces as are common in the reactions of nitrogenase at the FeMo-co catalytic site. The procedure (detailed in the ESI†) automatically moves down a ridge between minima to obtain the transition state.

3. Results

The thermodynamics of N_2 binding end-on at the *exo*-Fe2 position were calculated for the resting state and 19 intermediates along the mechanism pathway. The computational procedure first determines the transition state (TS) for N_2 binding, and then follows the trajectories from the TS to the associated and dissociated structures. Geometry and energy can be determined precisely for the associated structure and the transition state, but the limit of the dissociation trajectory has some uncertainty. The dissociation trajectory towards the N_2-pocket is tracked by monitoring the Fe2–N distance as well as structural changes in the FeMo-co cluster. These include the Fe2–C^c distance which responds to the *trans* Fe2–N interaction, together with the coupled Fe6–C^c distance. An important parameter is the *endo* angle at Fe2 (angle S2B–Fe2–S2A, specifically identified on Fig. 1) which varies according to the contents (*i.e.* H, N_2H_x, NH_y) of the intermediate, and also can change substantially as N_2 moves into the N_2-pocket. When it reaches the pocket, N_2 starts to tumble at an Fe2–N distance ranging 3.1 to 3.3 Å. As a consequence of these variabilities, the energy of the dissociated state is less certain, and because it affects the calculated association energy and the calculated association barrier these two potential energies are quoted at 1 kcal mol^{-1} precision. At the H_2/N_2 exchange stage of the mechanism there are two unbound molecules, H_2 and reducible N_2, in addition to non-reducible N_2, and therefore the calculation of trajectories required additional constraints in the computational model: the positions of H_2 and reducible N_2 were fixed.

Scheme 2 displays the calculated potential energies for the binding of N_2 from the N_2-pocket to *exo*-Fe2 coordination, colour coded as green when negative and blue when positive, together with the potential energy barrier for N_2 binding. The intermediates are sequenced according to the mechanism in Scheme 1, from the resting state, through 19 intermediates, and returning to the resting state. There are more than 19 intermediates in the complete mechanism, because each addition of an H atom involves several intermediates as H

Table 1 Calculated distances (Å) for the resting state of FeMo-co, for unprotonated and protonated forms of His195, in comparison with the crystallographic distances (PDB 3U7Q). Basis set DNP, functional PBE, S = 3/2, electronic state 235

Distance	xtl 3U7Q	Calculated with His195 unprotonated	Calc–xtl	Calculated with Hs195 protonated	Calc–xtl
Mean Fe–Fe	2.627	2.636	**0.009**	2.636	**0.009**
Mean Fe–S	2.231	2.233	**0.002**	2.240	**0.010**
Mean Fe–Mo	2.694	2.710	**0.016**	2.716	**0.022**
Mean C^c–Fe	1.999	1.993	**−0.006**	1.995	**−0.004**

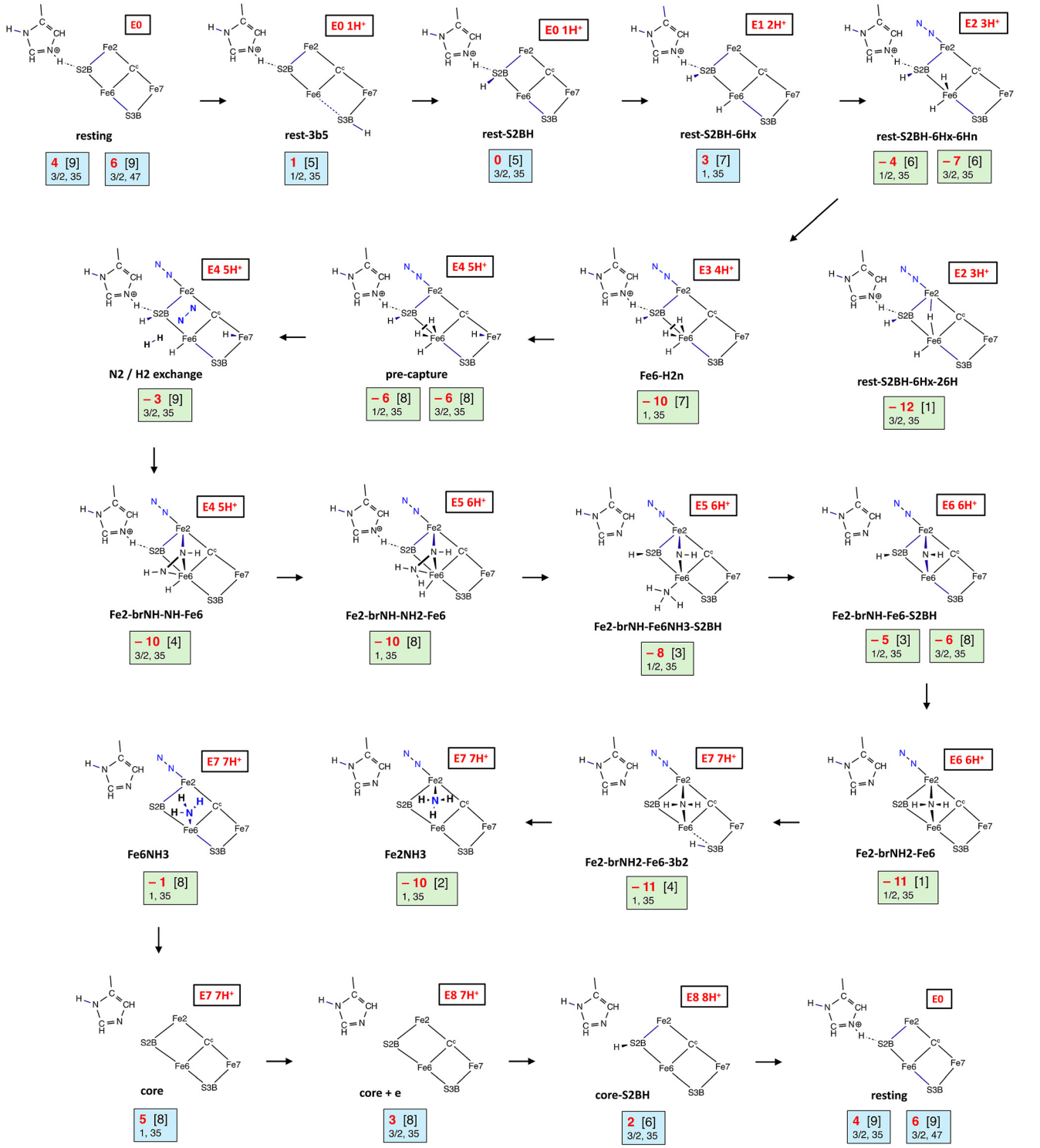

Scheme 2 The principal intermediates of the complete mechanism, in sequence, with the calculated potential energies (kcal mol^{-1}) for N_2 binding end-on at *exo*-Fe2 from the N_2-pocket in the protein. Each box contains the association potential energy in red, the barrier energy in parentheses, the spin state and the electronic state. The electron–proton status of each intermediate is marked. Blue boxes signify positive N_2 binding energy: green boxes signify negative N_2 binding energy. Structural skeletons include *exo*-Fe2–N_2 where the binding is favourable. Structure **rest-S2BH-6Hx-26H** is bypassed in the mechanism but is included here to demonstrate the effect of the bridging ligand on the *exo*-Fe2–N_2 binding thermodynamics. The pathway from **Fe2-brNH2-Fe6-3b2** to **core** could be *via* **Fe2NH3** or **Fe6NH3**. Informative pictures of the structures are included in the ESI.†

migrates from S3B to a target position on the active face, or to an N atom. However it became evident that it was not necessary to calculate the *exo*-Fe–N_2 association thermodynamics for all intermediates because there are patterns in the results which reveal the probable thermodynamics for all intermediates. This pattern is described in section 3.1.

The resting state and the first intermediates that follow, adding H atoms first at S2B, then at *exo*-Fe6 (**rest-S2BH-6Hx**), have positive binding energies for *exo*-Fe2–N_2, but after the third H is added at the *endo*-Fe6 position (**rest-S2BH-6Hx-6Hn**), this binding energy becomes negative. If the third H instead bridges Fe6 and Fe2 (**rest-S2BH-6Hx-26H**) the binding energy is −12 kcal mol^{-1} with a small association barrier of 1 kcal mol^{-1}. Negative *exo*-Fe2–N_2 binding energies continue for the subsequent intermediates, first the formation of H_2 (**Fe6-H2n**), then **pre-capture**, then the H_2/N_2 exchange (**H2/N2 exchange**), capture of N_2 with formation of the HNNH intermediate (**Fe2-brNH-NH-Fe6**, then **Fe2-brNH2-NH-Fe6**), after breaking N–N (**Fe2-brNH-Fe6NH3-S2BH**), after dissociation of NH_3 from Fe6 and then on to formation of **Fe2-brNH2-Fe6–3b2**. The subsequent formation of the second NH_3 could occur at Fe2 or Fe6, and these two intermediates have distinctly different binding thermodynamics and kinetics for N_2 at *exo*-Fe2: −10[2] kcal mol^{-1} for **Fe2NH3** and −1[8] kcal mol^{-1} for **Fe6NH3**. After dissociation of this NH_3, the intermediate **core** and the following intermediates that recover the resting state have positive N_2 binding energies. For all of the intermediates with negative binding energies the potential energy barriers to N_2 binding at *exo*-Fe2 are small, ≤8 kcal mol^{-1} and the barriers for dissociation of this N_2 range 11 to 18 kcal mol^{-1}.

The main pattern evident in these results is that intermediates with ligation at the *endo* position of Fe2 have favourable thermodynamics for binding N_2 at *exo*-Fe2. Three intermediates, **Fe6-H2n**, **pre-capture** and **N2/H2 exchange** do not have an *endo*-Fe2 bond but have negative binding energies for *exo*-Fe2–N_2, and this is correlated with a modification of the geometric details of FeMo-co caused by abnormally long Fe6–C^c distances (2.2–2.3 Å) in these intermediates. Overall the pattern of results validates the assumption that in the central stages of the mechanism, from **rest-S2BH-6Hx-6Hn** to **core**, the *exo*-Fe2–N_2 binding energies will be negative, and also negative in the intermediates involving the reconfigurations of incoming H atoms around S3B and migrations to other sites, because these steps do not interfere with ligation at *endo*-Fe2.

3.1. Bonding interpretation

The results above show that the binding energy for N_2 at *exo*-Fe2 is negative when there is ligation at the *endo*-Fe2 position, and positive when this ligation is absent. The difference between **Fe2NH3** (five-coordinate at Fe2, ΔE −10 kcal mol^{-1}) and **Fe6NH3** (four-coordinate at Fe2, ΔE −1 kcal mol^{-1}) exemplifies this property. This preference for additional coordination (at *exo*-Fe2) in a site with larger coordination number (*endo*-Fe2 ligation) is contrary to the general expectation from coordination chemistry that additional coordination is favoured at a site with a smaller coordination number. The data in Fig. 3 provide some insight into the bonding interpretation of the apparently anomalous binding of N_2 at *exo*-Fe2. The key geometric property is the *endo* angle at Fe2 (S2B–Fe2–S2A), which varies considerably over the range of intermediates in the mechanism. Fig. 3 reveals separation of two groups of structures. Looking at the geometry of the dissociated structures (black circles), in one group (lavender colouration) the *endo* angle is *ca.* 120° and the stereochemistry at four-coordinate Fe2 is essentially trigonal pyramidal (as in the resting state). These structures have positive or small negative N_2 binding energies. Intermediates in the other group (yellow colouration) have distinctly larger *endo* angles as a consequence of a ligand (H or N) bound at the *endo* position, and so these dissociated forms have pseudo-square pyramidal coordination. For these the N_2 binding energy is favourably negative. The general property of almost all intermediates is that square-pyramidal five coordinate Fe2 binds N_2 to form pseudo-octahedral Fe2 more favourably than trigonal pyramidal four coordinate Fe2 binds N_2 to form pseudo-trigonal bipyramidal five coordinate Fe2. On Fig. 3 the labelled structures outside the lavender and yellow fields have ligands near the *endo* position of Fe2, but not bound to Fe2, allowing relatively small *endo* angles. These structures, which occur in the intermediates just prior to the N_2-capture phase of the mechanism, retain significantly negative N_2 binding energies. Fig. 3 also plots the *endo* angles in the corresponding structures with *exo*-Fe2–N_2 bound, and in all intermediates the *endo* angle increases (vertical red–black separations) with *exo*-Fe2–N_2 coordination. Note that in the favourably bound intermediates (yellow enclosure) the *endo* angles range upwards of 160° and the coordination stereochemistry of Fe2 is therefore close to octahedral.

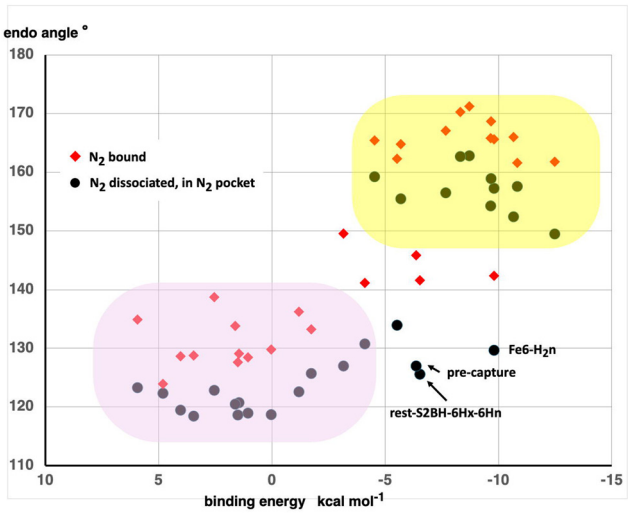

Fig. 3 Relationships between the binding energy for N_2 at *exo*-Fe2 (kcal mol^{-1}) and the *endo* angle (°) at Fe2, S2B–Fe2–S2A, for the dissociated (black circles) and associated (red diamond) forms of each of the intermediates. Data pairs for each intermediate are linked vertically.

4. Discussion

4.1. Entropy

The binding of N_2 to FeMo-co involves a loss of entropy, and this penalty needs to be considered with the binding potential energies calculated here in assessing the viability of N_2 binding at *exo*-Fe2. Quantum calculation of this entropy change is not feasible for a large model containing sufficient protein. However, relevant experimental data are available and can be assessed in the framework of Scheme 3. The datum sought here is ΔS^{assoc}, for the binding of N_2 in the N_2 approach pocket of the protein to Fe of FeMo-co in the protein. Values for ΔS^{model} are available from measurements of N_2 binding to model complexes that have chemical similarities with the Fe sites of FeMo-co.[97,98] Data on the solubility of N_2 in various solvents yield values for ΔS^{soln}. With several assumptions ΔS^{assoc} can be approximated as the difference ΔS^{model}–ΔS^{soln}. The assumption that N_2–M bonding in the model complexes is similar to N_2–Fe2 bonding at FeMo-co is valid, as is the assumption that the influences of surrounds in the *bound* state, solution *vs.* protein, are very similar. The assumed similarity of N_2 in solution and N_2 in the protein pocket is less valid, given the difference in fluidity of the two condensed phases and the expected larger librational component of the entropy of N_2 in solution.

The data are in Table 2, and possess good consistency: ΔS^{soln} varies little for very different solvents. Average values −33 cal mol^{-1} K^{-1} for ΔS^{model} and −13 cal mol^{-1} K^{-1} for ΔS^{soln}, yield ΔS^{assoc} = −20 cal mol^{-1} K^{-1}, so that $-T\Delta S^{assoc}$ calculates as 6 kcal mol^{-1}. With the expectation that the entropy of N_2 *in proteo* is more negative than that of N_2 in fluid solution, the conclusion is that $-T\Delta S^{assoc}$ for N_2 in the protein is considerably less than 6 kcal mol^{-1}. Henchman and Irudayam report theoretical investigations of the entropic cost of small molecule binding in proteins, with a comprehensive discussion of other experimental and theoretical information.[99] None of the systems calculated there closely resemble N_2 in the nitrogenase protein, but it is worth noting that benzene within a small protein (T4-lysozyme) is calculated to have lost between −16 and −23 cal mol^{-1} K^{-1}. If an entropy loss of this magnitude is applied instead of −13 cal mol^{-1} K^{-1} for ΔS^{soln}, $-T\Delta S^{assoc}$ for N_2 in the protein is *ca.* 4 kcal mol^{-1}.

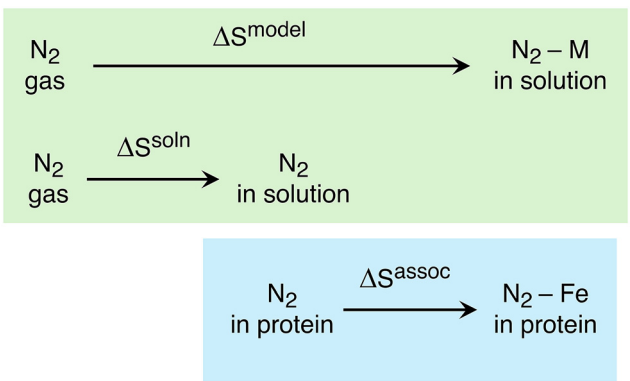

Scheme 3 Components of the analysis of entropy changes.

Seefeldt, Peters *et al.* described the structure and dynamics of a modified MoFe protein (96Arg → Gln) containing an acetylene molecule in a pocket near the front face of FeMo-co but not bound to it.[47] They suggested that acetylene in the protein channel leading to its pocket has practically lost most of its gas phase entropy content.

After application of a $-T\Delta S$ penalty of no more than 4 kcal mol^{-1} to the intermediates in Scheme 2 that have a negative potential energy for binding of N_2 at *exo*-Fe2, all intermediates except two are calculated to have a negative free energy for this binding. The exceptions are **N2/H2 exchange** (ΔG *ca.* +1 kcal mol^{-1}) and **Fe6NH3** (ΔG *ca.* +3 kcal mol^{-1}). As mentioned above the calculation of ΔE for **N2/H2 exchange** is less reliable than others, because three unbound molecules are involved, and therefore it is uncertain whether *exo*-Fe2–N_2 would dissociate at this stage in the mechanism. The next intermediate in the mechanism sequence, **Fe2-brNH-NH-Fe6**, certainly contains *exo*-Fe2–N_2 (ΔG *ca.* −6 kcal mol^{-1}).

It is assumed in this report and in my other accounts of aspects of the mechanism that any transfer of non-reducible N_2 between the N_2-pocket and the *exo*-Fe2 position is a process separate from the reaction steps from one intermediate to the next. It is conceivable that these processes could be concerted, but the conclusion that all intermediates from **rest-S2BH-6Hx-6Hn** to **core** have negative free energies for N_2 binding at *exo*-Fe2 suggests that this is unlikely.

4.2. Connecting with experiment

None of the experimental structures of the FeMo protein shows N_2 bound at the *exo*-Fe2 position, although the crystallisation systems used may not have contained N_2. The compu-

Table 2 Entropy data in cal mol^{-1} K^{-1}

System	ΔS^{model}	ΔS^{soln}	Ref.
$[P(C_6H_{11})_3]_2Cr(CO)_3$ in THF, 5.1 atm N_2	−35.4 ± 2.3		97
$[P(C_6H_{11})_3]_2Mo(CO)_3$ in THF, 1 atm N_2	−32.1 ± 3.2		97
(TPB)Co(N_2) in toluene, 1 atm N_2	−32(5)		98
Dissolved in cyclohexane, 1 atm N_2		−11.1	100
Dissolved in *n*-decane, 1 atm N_2		−13.6	101
Dissolved in 1-octanol, 1 atm N_2		−12.7	101
Dissolved in octamethylcyclotetrasiloxane, 1 atm N_2		−11.6	102
CCl_4		−12.6	Quoted in ref. 103
Dissolved in ethanol plus 2-propanone (0.558 mol fraction ethanol)		−13.8	Ref. 104, quoted in ref. 103
Ethanol plus 2,2,4-trimethylpentane (0.739 mol fraction ethanol)		−13.9	Ref. 104, quoted in ref. 103

tational results here are consistent with this absence, because the binding potential energy in the resting state is calculated to be *ca*. +5 kcal mol^{-1}, and the entropy component makes the free energy change more positive. In the absence of definitive structures of intermediates in the central stages of the mechanism, obtained by crystallisation and diffraction, or by cryoEM,[4,105] how might experimental support for the proposed binding of N_2 at *exo*-Fe2 be sought?

One general approach in mechanistic studies is to mutate key residues in order to block the postulated function and diminish or prevent the outcome of the mechanism. In the present context this would involve modifying residues at some of the positions 278, 281, 277, 196, 383. However, because it has not yet been demonstrated computationally that any of the mechanistic steps in Scheme 1 is energetically too difficult when *exo*-Fe2–N_2 is absent, this strategy could be inconclusive. Calculations of the thermodynamics and viability of the mechanistic steps when *exo*-Fe2–N_2 is absent are still to be finalised. Uncertainty arises from the proposed dual roles of N_2. Simply put, if a blocking mutation inhibits NH_3 formation, is that due to a blockage of reducible N_2 reaching the reaction zone, or a blocked formation of *exo*-Fe2–N_2 required to promote one or more steps in the mechanism?

There is another factor. An alternative N_2 ingress channel has been proposed by Morrison *et al*. based on the locations of Xe atoms trapped in the MoFe protein (PDB 4WNA), together with the generation of potential substrate pathways using the program CAVER.[106] The results relevant here are shown in Fig. 4 (which is Fig. 3a in ref. 106) The Morrison pathway for substrates approaching the Fe2–Fe3–Fe6–Fe7 face of FeMo-co is the slate blue channel in Fig. 4. This channel extends from the Xe1 location which is 13 Å from Fe2. Fig. 5 shows the

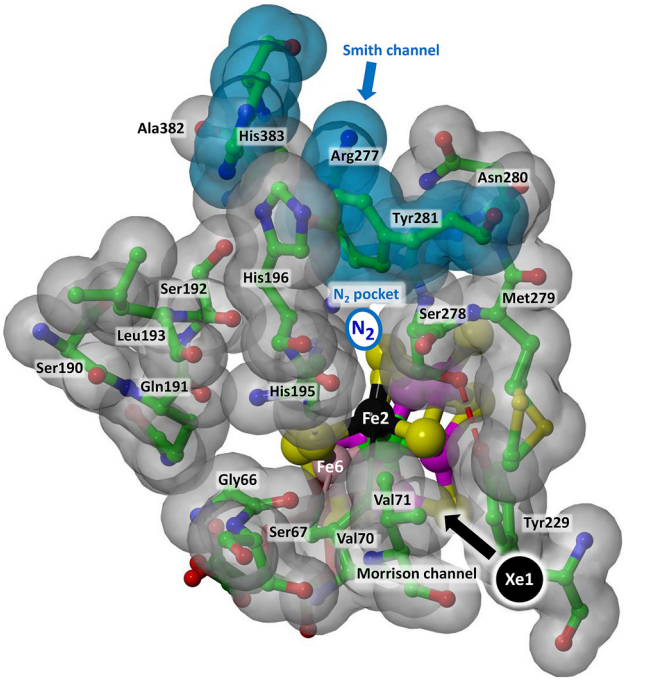

Fig. 5 The different positions and directions of the Smith channel[51] and the Morrison channel.[106]

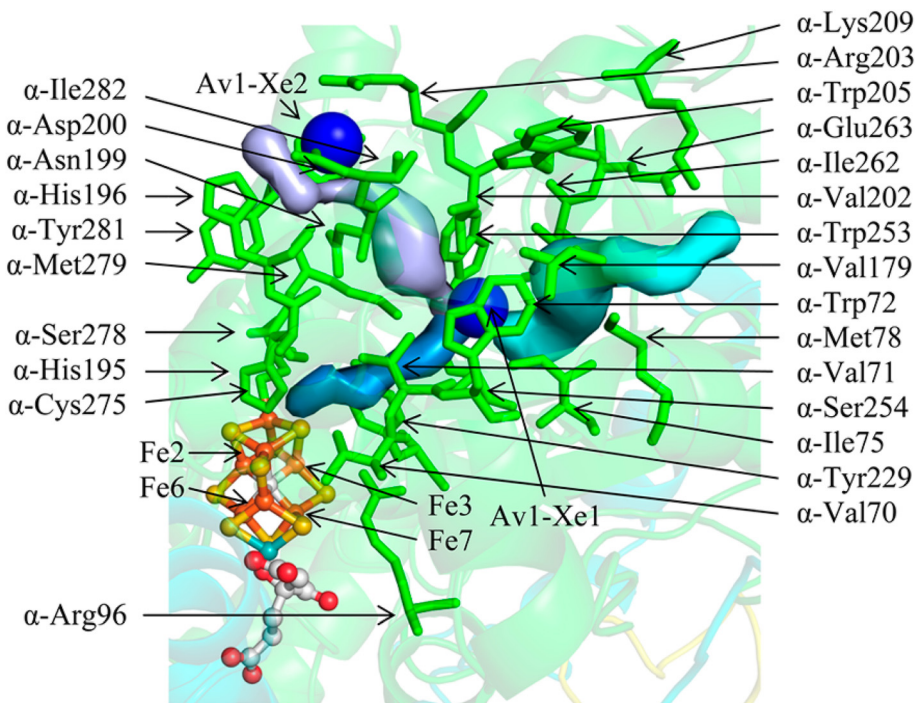

Fig. 4 Locations of Xe atoms in *Av* MoFe protein crystal PDB 4WNA and substrate channels calculated with the program CAVER: reproduced with permission from ref. 106. The light purple and cyan pathways connect the protein surface to the Xe1 site, from which substrate N_2 could continue towards the Fe2–Fe3–Fe6–Fe7 face of FeMo-co through the slate blue channel, and enter the reaction zone.

location of Xe1 and the direction of the Morrison channel drawn on the scenario of Fig. 2: the original ingress channel is labeled as Smith channel. It is obvious that these are two different pathways for the ingress of N_2. I have already shown that reducible N_2 can diffuse around bound non-reducible N_2,[66] but it is conceivable that the N_2 which is reduced in the reaction zone according to Scheme 1 enters along the Morrison pathway while the N_2 that binds at *exo*-Fe2 from the N2-pocket enters along the Smith pathway. Mutagenesis experimentation would need to target both of these pathways. Further speculation has limited value at this time. A definitive experimental structure of an intermediate in the Mo–nitrogenase physiological reaction is needed for direct confirmation of the presence of *exo*-Fe2–N_2.

4.3. The role of S2B

The mechanism in Scheme 1 involves a catalytic site, FeMo-co, that is structurally flexible but with intact intra-cluster bonding. In recent years the structural integrity of FeMo-co during catalysis has been questioned by the crystal structures and reactivities of Mo–nitrogenase isoforms in which S2B has been replaced by Se,[107] or CO,[108,109] or, controversially, by N_2.[110–113] The mechanistic relevance of these findings is unresolved, because the apparent displacement or replacement of S2B could reflect different dynamics between the time scales of substrate reduction and crystal growth.[4]

In my analyses of the mechanism, S2B is retained within intact FeMo-co, and in that position has crucial roles in which an H atom on S2B is used to form an H–N bond. One role is the N_2 capture step forming **Fe2-brNH-NH-Fe6**, and the second is the **Fe2-brNH-Fe6-S2BH → Fe2-brNH2-Fe6** step. In both steps S2BH is needed to form an H–N bond on the His195 side of the reaction zone, and throughout the mechanism His195 functions as proton reservoir and proton buffer (evident in Scheme 1 Panel B and the recovery of the resting state in Panel C) *via* contact with S2B very similar in distance (*ca.* 3.2 Å) to the resting state crystal structure. Many components of the proposed mechanism would be invalidated if S2B were absent.

5. Conclusions

This investigation has clarified and quantified the occurrence of a non-reducible N_2 molecule in the proposed complete mechanism of Mo–nitrogenase. In the resting state this N_2 will occupy the N_2-pocket about 3.2 Å from Fe2. After introduction of three H atoms at positions surrounding the reaction zone this non-reducible N_2 will relocate to the *exo* position of Fe2 with end-on coordination. A separate (reducible) N_2 entering the reaction zone is progressively hydrogenated, through intermediates containing N_2H_x and NH_x entities coordinated at the *endo* position of Fe2, and this *endo*-Fe2 coordination favours retention of the *exo*-Fe2–N_2 moiety through this sequence of intermediates. In the last stages of the mechanism after dissociation of the second NH_3 and clearance of the *endo*-Fe position the thermodynamics favour return of non-reducible N_2 to the N_2-pocket. Some uncertainty remains about the status of *exo*-Fe2–N_2 during one step in which H_2 exchanges with the incoming reducible N_2.

Coordination at *endo*-Fe2 is confirmed as a structural feature that favours binding of N_2 at *exo*-Fe2, and attainment of pseudo-octahedral stereochemistry at Fe2 is evidently the dominant factor explaining the apparent paradox in which binding at the *exo* position of Fe2 is enabled by ligation at the *endo* position of the same Fe atom.

These results also justify the assumed presence of *exo*-Fe2–N_2 in the models used in previous calculations of the thermochemistry of mechanistic reaction steps.[52,53] The appropriate presence or absence of *exo*-Fe2–N_2 for each of the intermediates is included in the Scheme 1 presentation of the full mechanism. A central hypothesis is that *exo*-Fe2–N_2 is non-reducible because it is outside the reaction zone and not exposed to H atom donors.

For the resting state the binding free energy for *exo*-Fe2–N_2 is calculated to be *ca.* +9 kcal mol^{-1}, which is consistent with the absence of N_2 at Fe2 in all reported crystal structures of the MoFe protein.

Data availability

The data supporting this article have been included as part of the ESI.†

Electronic supplementary information (ESI) available: Description of the protein model and the structural constraints used, explanation of the electronic states, description of the density functional procedures and their validation, and description of procedures for determination of transition states and reaction trajectories. Atom coordinates, spin densities of Fe atoms, and pictorial representations of all structures and transition states are included in the ESI.†

Conflicts of interest

There are no conflicts to declare.

Acknowledgements

This research was undertaken with the aid of resources from the National Computational Infrastructure Facility, enabled by the Australian Government. My research is funded by UNSW Sydney.

References

1 A. K. Garcia, D. F. Harris, A. J. Rivier, B. M. Carruthers, A. Pinochet-Barros, L. C. Seefeldt and B. Kaçar, Nitrogenase resurrection and the evolution of a singular enzymatic mechanism, *eLife*, 2023, **12**, e85003, DOI: 10.7554/eLife.85003.

2 V. Smil, *Enriching the Earth: Fritz Haber, Carl Bosch, and the Transformation of World Food Production*, MIT Press, Cambridge, Massachusetts, 2001.
3 S. D. Threatt and D. C. Rees, Biological nitrogen fixation in theory, practice, and reality: a perspective on the molybdenum nitrogenase system, *FEBS Lett.*, 2022, **597**, 45–58, DOI: 10.1002/1873-3468.14534.
4 R. A. Warmack and D. C. Rees, Nitrogenase beyond the Resting State: A Structural Perspective, *Molecules*, 2023, **28**, 7952, DOI: 10.3390/molecules28247952.
5 R. N. F. Thorneley and D. J. Lowe, in *Molybdenum enzymes*, ed. T. G. Spiro, Wiley Interscience, New York, 1985, ch. 5, pp. 221–284.
6 D. F. Harris, A. Badalyan and L. C. Seefeldt, Mechanistic Insights into Nitrogenase FeMo-Cofactor Catalysis through a Steady-State Kinetic Model, *Biochemistry*, 2022, **61**, 2131–2137, DOI: 10.1021/acs.biochem.2c00415.
7 B. M. Barney, R. Y. Igarashi, P. C. Dos Santos, D. R. Dean and L. C. Seefeldt, Substrate Interaction at an Iron-Sulfur Face of the FeMo-cofactor during Nitrogenase Catalysis, *J. Biol. Chem.*, 2004, **279**, 53621–53624.
8 R. Sarma, B. M. Barney, S. Keable, D. R. Dean, L. C. Seefeldt and J. W. Peters, Insights into substrate binding at FeMo-cofactor in nitrogenase from the structure of an a-70Ile MoFe protein variant, *J. Inorg. Biochem.*, 2010, **104**, 385–389.
9 D. J. Scott, H. D. May, W. E. Newton, K. E. Brigle and D. R. Dean, Role for the nitrogenase MoFe protein [alpha]-subunit in FeMo-cofactor binding and catalysis, *Nature*, 1990, **343**, 188–190.
10 C. H. Kim, W. E. Newton and D. R. Dean, Role of the MoFe protein alpha subunit histidine-195 residue in FeMo-cofactor binding and nitrogenase catalysis, *Biochemistry*, 1995, **34**, 2798–2808.
11 M. J. Dilworth, K. Fisher, C. H. Kim and W. E. Newton, Effects on substrate reduction of substitution of histidine-195 by glutamine in the alpha-subunit of the MoFe protein of Azotobacter vinelandii nitrogenase, *Biochemistry*, 1998, **37**, 17495–17505.
12 K. Fisher, M. J. Dilworth and W. E. Newton, Differential Effects on N_2 Binding and Reduction, HD Formation, and Azide Reduction with a-195His- and a-191Gln-Substituted MoFe Proteins of Azotobacter Vinelandii Nitrogenase, *Biochemistry*, 2000, **39**, 15570–15577.
13 Z.-Y. Yang, K. Danyal and L. C. Seefeldt, Mechanism of Mo-Dependent Nitrogenase, *Methods Mol. Biol.*, 2011, **766**, 9–29.
14 K. Fisher, M. J. Dilworth, C.-H. Kim and W. E. Newton, Azotobacter Vinelandii Nitrogenases Containing Altered MoFe Proteins with Substitutions in the FeMo-Cofactor Environment: Effects on the Catalyzed Reduction of Acetylene and Ethylene, *Biochemistry*, 2000, **39**, 2970–2979.
15 J. Christiansen, V. L. Cash, L. C. Seefeldt and D. R. Dean, Isolation and characterisation of an acetylene-resistant nitrogenase, *J. Biol. Chem.*, 2000, **275**, 11459–11464.
16 J. Christiansen, L. C. Seefeldt and D. R. Dean, Competitive Substrate and Inhibitor Interactions at the Physiologically Relevant Active Site of Nitrogenase, *J. Biol. Chem.*, 2000, **275**, 36104–36107.
17 Z. Maskos, K. Fisher, M. Sorlie, W. E. Newton and B. J. Hales, Variant MoFe proteins of Azotobacter vinelandii: effects of carbon monoxide on electron paramagnetic resonance spectra generated during enzyme turnover, *J. Biol. Inorg. Chem.*, 2005, **10**, 394–406.
18 B. M. Barney, D. Lukoyanov, T.-C. Yang, D. R. Dean, B. M. Hoffman and L. C. Seefeldt, A methyldiazene ($HN{=}N{-}CH_3$)-derived species bound to the nitrogenase active-site FeMo cofactor: Implications for mechanism, *Proc. Natl. Acad. Sci. U. S. A.*, 2006, **103**, 17113–17118.
19 P. C. Dos Santos, S. M. Mayer, B. M. Barney, L. C. Seefeldt and D. R. Dean, Alkyne substrate interaction within the nitrogenase MoFe protein, *J. Inorg. Biochem.*, 2007, **101**, 1642–1648.
20 K. Fisher, D. J. Lowe, P. Tavares, A. S. Pereira, B. H. Huynh, D. Edmondson and W. E. Newton, Conformations generated during turnover of the Azotobacter vinelandii nitrogenase MoFe protein and their relationship to physiological function, *J. Inorg. Biochem.*, 2007, **101**, 1649–1656.
21 L. B. Gee, A. D. Scott, C. H. Dapper, W. E. Newton and S. P. Cramer, Carbon monoxide binding to α-R277H Mo-nitrogenase – Evidence for multiple pH-dependent species from IR-monitored photolysis, *J. Inorg. Biochem.*, 2022, **232**, 111806, DOI: 10.1016/j.jinorgbio.2022.111806.
22 A. D. Scott, V. Pelmenschikov, Y. Guo, L. Yan, H. Wang, S. J. George, C. H. Dapper, W. E. Newton, Y. Yoda, Y. Tanaka and S. P. Cramer, Structural Characterization of CO-Inhibited Mo-Nitrogenase by Combined Application of NRVS, EXAFS, and DFT: New Insights into the Effects of CO Binding and the Role of the Interstitial Atom, *J. Am. Chem. Soc.*, 2014, **136**, 15942–15954, DOI: 10.1021/ja505720m.
23 M. Maiuri, I. Delfino, G. Cerullo, C. Manzoni, V. Pelmenschikov, Y. Guo, H. Wang, L. B. Gee, C. H. Dapper, W. E. Newton and S. P. Cramer, Low frequency dynamics of the nitrogenase MoFe protein via femtosecond pump probe spectroscopy—Observation of a candidate promoting vibration, *J. Inorg. Biochem.*, 2015, **153**, 128–135, DOI: 10.1016/j.jinorgbio.2015.07.005.
24 L. B. Gee, H. Wang and S. P. Cramer, in *Methods in Enzymology*, ed. S. S. David, Academic Press, 2018, vol. 599, pp. 409–425.
25 V. Hoeke, L. Tociu, D. A. Case, L. C. Seefeldt, S. Raugei and B. M. Hoffman, High-Resolution ENDOR Spectroscopy Combined with Quantum Chemical Calculations Reveals the Structure of Nitrogenase Janus Intermediate E4(4H), *J. Am. Chem. Soc.*, 2019, **141**, 11984–11996, DOI: 10.1021/jacs.9b04474.
26 C. Van Stappen, L. Decamps, G. E. Cutsail, R. Bjornsson, J. T. Henthorn, J. A. Birrell and S. DeBeer, The Spectroscopy of Nitrogenases, *Chem. Rev.*, 2020, **120**, 5005–5081, DOI: 10.1021/acs.chemrev.9b00650.

27 L. Deng, H. Wang, C. H. Dapper, W. E. Newton, S. Shilov, S. Wang, S. P. Cramer and Z.-H. Zhou, Assignment of protonated R-homocitrate in extracted FeMo-cofactor of nitrogenase via vibrational circular dichroism spectroscopy, *Commun. Chem.*, 2020, **3**, 145, DOI: **10.1038/s42004-020-00392-z**.

28 A. Pérez-González, Z.-Y. Yang, D. A. Lukoyanov, D. R. Dean, L. C. Seefeldt and B. M. Hoffman, Exploring the Role of the Central Carbide of the Nitrogenase Active-Site FeMo-cofactor through Targeted ^{13}C Labeling and ENDOR Spectroscopy, *J. Am. Chem. Soc.*, 2021, **143**, 9183–9190, DOI: **10.1021/jacs.1c04152**.

29 D. A. Lukoyanov, D. F. Harris, Z.-Y. Yang, A. Pérez-González, D. R. Dean, L. C. Seefeldt and B. M. Hoffman, The One-Electron Reduced Active-Site FeFe-Cofactor of Fe-Nitrogenase Contains a Hydride Bound to a Formally Oxidized Metal-Ion Core, *Inorg. Chem.*, 2022, **61**, 5459–5464, DOI: **10.1021/acs.inorgchem.2c00180**.

30 D. A. Lukoyanov, Z. Y. Yang, A. Perez-Gonzalez, S. Raugei, D. R. Dean, L. C. Seefeldt and B. M. Hoffman, C-13 ENDOR Characterization of the Central Carbon within the Nitrogenase Catalytic Cofactor Indicates That the CFe6 Core Is a Stabilizing "Heart of Steel", *J. Am. Chem. Soc.*, 2022, **144**, 18315–18328, DOI: **10.1021/jacs.2c06149**.

31 T. Spatzal, M. Aksoyoglu, L. Zhang, S. L. A. Andrade, E. Schleicher, S. Weber, D. C. Rees and O. Einsle, Evidence for Interstitial Carbon in Nitrogenase FeMo Cofactor, *Science*, 2011, **334**, 940.

32 O. Einsle and D. C. Rees, Structural Enzymology of Nitrogenase Enzymes, *Chem. Rev.*, 2020, **120**, 4969–5004, DOI: **10.1021/acs.chemrev.0c00067**.

33 H. L. Rutledge, B. D. Cook, H. P. M. Nguyen, M. A. Herzik and F. A. Tezcan, Structures of the nitrogenase complex prepared under catalytic turnover conditions, *Science*, 2022, **377**, 865–869, DOI: **10.1126/science.abq7641**.

34 S. Raugei, L. C. Seefeldt and B. M. Hoffman, Critical computational analysis illuminates the reductive-elimination mechanism that activates nitrogenase for N_2 reduction, *Proc. Natl. Acad. Sci. U. S. A.*, 2018, **115**, E10521–E10530, DOI: **10.1073/pnas.1810211115**.

35 A. T. Thorhallsson, B. Benediktsson and R. Bjornsson, A model for dinitrogen binding in the E4 state of nitrogenase, *Chem. Sci.*, 2019, **10**, 11110–11124, DOI: **10.1039/C9SC03610E**.

36 I. Dance, Survey of the geometric and electronic structures of the key hydrogenated forms of FeMo-co, the active site of the enzyme nitrogenase: principles of the mechanistically significant coordination chemistry, *Inorganics*, 2019, **7**, 8, DOI: **10.3390/inorganics7010008**.

37 I. Dance, Computational Investigations of the Chemical Mechanism of the Enzyme Nitrogenase, *ChemBioChem*, 2020, **21**, 1671–1709, DOI: **10.1002/cbic.201900636**.

38 L. Cao and U. Ryde, What Is the Structure of the E4 Intermediate in Nitrogenase?, *J. Chem. Theory Comput.*, 2020, **16**, 1936–1952, DOI: **10.1021/acs.jctc.9b01254**.

39 I. Dance, Structures and reaction dynamics of N_2 and H_2 binding at FeMo-co, the active site of nitrogenase, *Dalton Trans.*, 2021, **50**, 18212–18237, DOI: **10.1039/d1dt03548g**.

40 A. T. Thorhallsson and R. Bjornsson, The E2 state of FeMoco: Hydride Formation versus Fe Reduction and a Mechanism for H_2 Evolution, *Chem. – Eur. J.*, 2021, **27**, 16788–16800, DOI: **10.1002/chem.202102730**.

41 H. Jiang and U. Ryde, Thermodynamically Favourable States in the Reaction of Nitrogenase without Dissociation of any Sulfide Ligand, *Chem. – Eur. J.*, 2022, **28**, e202103933, DOI: **10.1002/chem.202103933**.

42 Y. Pang and R. Bjornsson, The E3 state of FeMoco: one hydride, two hydrides or dihydrogen?, *Phys. Chem. Chem. Phys.*, 2023, **25**, 21020–21036, DOI: **10.1039/D3CP01106B**.

43 Y. Pang and R. Bjornsson, Understanding the Electronic Structure Basis for N_2 Binding to FeMoco: A Systematic Quantum Mechanics/Molecular Mechanics Investigation, *Inorg. Chem.*, 2023, **62**, 5357–5375, DOI: **10.1021/acs.inorgchem.2c03967**.

44 R. N. F. Thorneley and D. J. Lowe, Nitrogenase - Substrate Binding and Activation, *J. Biol. Inorg. Chem.*, 1996, **1**, 576–580.

45 B. M. Barney, H.-I. Lee, P. C. Dos Santos, B. M. Hoffman, D. R. Dean and L. C. Seefeldt, Breaking the N_2 triple bond: insights into the nitrogenase mechanism, *Dalton Trans.*, 2006, 2277–2284, DOI: **10.1039/b517633f**.

46 L. C. Seefeldt, B. M. Hoffman and D. R. Dean, Mechanism of Mo-Dependent Nitrogenase, *Annu. Rev. Biochem.*, 2009, **78**, 701–722.

47 S. M. Keable, J. Vertemara, O. A. Zadvornyy, B. J. Eilers, K. Danyal, A. J. Rasmussen, L. De Gioia, G. Zampella, L. C. Seefeldt and J. W. Peters, Structural characterization of the nitrogenase molybdenum-iron protein with the substrate acetylene trapped near the active site, *J. Inorg. Biochem.*, 2018, **180**, 129–134, DOI: **10.1016/j.jinorgbio.2017.12.008**.

48 P. M. C. Benton, J. Christiansen, D. R. Dean and L. C. Seefeldt, Stereospecificity of Acetylene Reduction Catalyzed by Nitrogenase, *J. Am. Chem. Soc.*, 2001, **123**, 1822–1827.

49 P. C. Dos Santos, R. Igarashi, H.-I. Lee, B. M. Hoffman, L. C. Seefeldt and D. R. Dean, Substrate Interactions with the Nitrogenase Active Site, *Acc. Chem. Res.*, 2005, **38**, 208–214.

50 I. Dance, The pathway for serial proton supply to the active site of nitrogenase: enhanced density functional modeling of the Grotthuss mechanism, *Dalton Trans.*, 2015, **44**, 18167–18186, DOI: **10.1039/C5DT03223G**.

51 D. Smith, K. Danyal, S. Raugei and L. C. Seefeldt, Substrate Channel in Nitrogenase Revealed by a Molecular Dynamics Approach, *Biochemistry*, 2014, **53**, 2278–2285, DOI: **10.1021/bi401313j**.

52 I. Dance, The activating capture of N_2 at the active site of Mo–nitrogenase, *Dalton Trans.*, 2024, **53**, 14193–14211, DOI: **10.1039/d4dt01866d**.

53 I. Dance, The mechanism of Mo-nitrogenase: from N_2 capture to first release of NH_3, *Dalton Trans.*, 2024, **53**, 19360–19377, DOI: 10.1039/d4dt02606c.
54 T. M. Buscagan and D. C. Rees, Rethinking the Nitrogenase Mechanism: Activating the Active Site, *Joule*, 2019, **3**, 2662–2678, DOI: 10.1016/j.joule.2019.09.004.
55 L. C. Seefeldt, Z.-Y. Yang, D. A. Lukoyanov, D. F. Harris, D. R. Dean, S. Raugei and B. M. Hoffman, Reduction of Substrates by Nitrogenases, *Chem. Rev.*, 2020, **120**, 5082–5106, DOI: 10.1021/acs.chemrev.9b00556.
56 L. Cao and U. Ryde, Putative reaction mechanism of nitrogenase after dissociation of a sulfide ligand, *J. Catal.*, 2020, **391**, 247–259, DOI: 10.1016/j.jcat.2020.08.028.
57 H. Jiang, O. K. G. Svensson, L. Cao and U. Ryde, Proton Transfer Pathways in Nitrogenase with and without Dissociated S2B, *Angew. Chem., Int. Ed.*, 2022, **61**, e202208544, DOI: 10.1002/anie.202208544.
58 O. Einsle, Catalysis and structure of nitrogenases, *Curr. Opin. Struct. Biol.*, 2023, **83**, 102719, DOI: 10.1016/j.sbi.2023.102719.
59 P. E. M. Siegbahn, The mechanism for nitrogenase including all steps, *Phys. Chem. Chem. Phys.*, 2019, **21**, 15747–15759, DOI: 10.1039/C9CP02073J.
60 W. J. Wei and P. E. M. Siegbahn, A Mechanism for Nitrogenase Including Loss of a Sulfide, *Chemistry*, 2022, **28**, e202103745, DOI: 10.1002/chem.202103745.
61 P. E. M. Siegbahn, The mechanism for N_2 activation in the E4 – state of nitrogenase, *Phys. Chem. Chem. Phys.*, 2023, **25**, 23602–23613, DOI: 10.1039/D3CP02851H.
62 P. E. M. Siegbahn, How Protons Move in Enzymes—The Case of Nitrogenase, *J. Phys. Chem. B*, 2023, **127**, 2156–2159, DOI: 10.1021/acs.jpcb.2c08567.
63 P. E. M. Siegbahn, Computational Model Study of the Experimentally Suggested Mechanism for Nitrogenase, *J. Phys. Chem. B*, 2024, **128**, 985–989, DOI: 10.1021/acs.jpcb.3c07675.
64 H. Jiang and U. Ryde, Putative reaction mechanism of nitrogenase with a half-dissociated S2B ligand, *Dalton Trans.*, 2024, **53**, 11500–11513, DOI: 10.1039/D4DT00937A.
65 I. Dance, What triggers the coupling of proton transfer and electron transfer at the active site of nitrogenase?, *Dalton Trans.*, 2024, **53**, 7996–8004, DOI: 10.1039/d4dt00474d.
66 I. Dance, The binding of reducible N_2 in the reaction domain of nitrogenase, *Dalton Trans.*, 2023, **52**, 2013–2026, DOI: 10.1039/D2DT03599E.
67 I. Dance, Calculating the chemical mechanism of nitrogenase: new working hypotheses, *Dalton Trans.*, 2022, **51**, 12717–12728, DOI: 10.1039/d2dt01920e.
68 E. K. Jackson, G. W. Parshall and R. W. F. Hardy, Hydrogen Reactions of Nitrogenase. Formation of the Molecule HD by Nitrogenase and by an Inorganic Model, *J. Biol. Chem.*, 1968, **243**, 4952–4958.
69 J.-L. Li and R. H. Burris, Influence of pN_2 and pD_2 on HD Formation by Various Nitrogenases, *Biochemistry*, 1983, **22**, 4472–4480.
70 J. H. Guth and R. H. Burris, Inhibition of Nitrogenase-Catalyzed NH_3 Formation by H_2, *Biochemistry*, 1983, **22**, 5111–5122.
71 I. Dance, The HD Reaction of Nitrogenase: a Detailed Mechanism, *Chem. – Eur. J.*, 2023, **29**, e202202502, DOI: 10.1002/chem.202202502.
72 A. K. Garcia, H. McShea, B. Kolaczkowski and B. Kaçar, Reconstructing the evolutionary history of nitrogenases: Evidence for ancestral molybdenum-cofactor utilization, *Geobiology*, 2020, **18**, 394–411, DOI: 10.1111/gbi.12381.
73 B. Benediktsson and R. Bjornsson, QM/MM Study of the Nitrogenase MoFe Protein Resting State: Broken-Symmetry States, Protonation States, and QM Region Convergence in the FeMoco Active Site, *Inorg. Chem.*, 2017, **56**, 13417–13429, DOI: 10.1021/acs.inorgchem.7b02158.
74 L. Cao and U. Ryde, Influence of the protein and DFT method on the broken-symmetry and spin states in nitrogenase, *Int. J. Quantum Chem.*, 2018, **118**, e25627, DOI: 10.1002/qua.25627.
75 H. Jiang, O. K. G. Svensson and U. Ryde, QM/MM Study of Partial Dissociation of S2B for the E2 Intermediate of Nitrogenase, *Inorg. Chem.*, 2022, **61**, 18067–18076, DOI: 10.1021/acs.inorgchem.2c02488.
76 H. Jiang and U. Ryde, N_2 binding to the E0–E4 states of nitrogenase, *Dalton Trans.*, 2023, **52**, 9104–9120, DOI: 10.1039/D3DT00648D.
77 B. Delley, An all-electron numerical method for solving the local density functional for polyatomic molecules, *J. Chem. Phys.*, 1990, **92**, 508–517.
78 B. Delley, in *Modern density functional theory: a tool for chemistry*, ed. J. M. Seminario and P. Politzer, Elsevier, Amsterdam, 1995, vol. 2, pp. 221–254.
79 J. Baker, A. Kessi and B. Delley, The generation and use of delocalized internal coordinates in geometry optimization, *J. Chem. Phys.*, 1996, **105**, 192–212, DOI: 10.1063/1.471864.
80 B. Delley, From molecules to solids with the DMol3 approach, *J. Chem. Phys.*, 2000, **113**, 7756–7764.
81 J. Andzelm, R. D. King-Smith and G. Fitzgerald, Geometry optimization of solids using delocalized internal coordinates, *Chem. Phys. Lett.*, 2001, **335**, 321–326, DOI: 10.1016/S0009-2614(01)00030-6.
82 T. Todorova and B. Delley, Molecular Crystals: A Test System for Weak Bonding†, *J. Phys. Chem. C*, 2010, **114**, 20523–20530, DOI: 10.1021/jp1049759.
83 Y. Zhang, W. Pan and W. Yang, Describing van der Waals Interaction in diatomic molecules with generalized gradient approximations: The role of the exchange functional, *J. Chem. Phys.*, 1997, **107**, 7921–7925.
84 J. Andzelm, C. Kolmel and A. Klamt, Incorporation of solvent effects into density functional calculations of molecular energies and geometries, *J. Chem. Phys.*, 1995, **103**, 9312–9320.
85 A. Klamt, V. Jonas, T. Burger and J. C. W. Lohrenz, Refinement and Parametrization of COSMO-RS, *J. Phys. Chem. A*, 1998, **102**, 5074–5085.
86 B. Delley, The conductor-like screening model for polymers and surfaces, *Mol. Simul.*, 2006, **32**, 117–123.

87 R. S. Mulliken, Electronic population analysis on LCAO-MO molecular wavefunctions. II. Overlap populations, bond orders, and covalent bond energies, *J. Chem. Phys.*, 1955, **23**, 1833–1846.
88 I. Dance, Evaluations of the Accuracies of DMol3 Density Functionals for Calculations of Experimental Binding Enthalpies of N_2, CO, H_2, C_2H_2 at Catalytic Metal Sites, *Mol. Simul.*, 2018, **44**, 568–581, DOI: **10.1080/08927022.2017.1413711**.
89 M. Meunier, N. Quirke and D. Binesti, The calculation of the electron affinity of atoms and molecules, *Mol. Simul.*, 1999, **23**, 109–125.
90 B. Delley, Ground-State Enthalpies: Evaluation of Electronic Structure Approaches with Emphasis on the Density Functional Method, *J. Phys. Chem. A*, 2006, **110**, 13632–13639, DOI: **10.1021/jp0653611**.
91 I. Dance, Understanding structure and reactivity of new fundamental inorganic molecules: metal sulfides, metallocarbohedrenes, and nitrogenase, *J. Chem. Soc., Chem. Commun.*, 1998, 523–530.
92 D. Schaniel, T. Wolke, B. Delley, C. Boskovic and H. U. Gudel, Photogeneration of metastable side-on N_2 linkage isomers in $[Ru(NH_3)_5N_2]Cl_2$, $[Ru(NH_3)_5N_2]Br_2$ and $[Os(NH_3)_5N_2]Cl_2$, *Phys. Chem. Chem. Phys.*, 2008, **10**, 5531–5538, DOI: **10.1039/b806933f**.
93 T. Todorova and B. Delley, The Creutz–Taube Complex Revisited: DFT Study of the Infrared Frequencies, *Inorg. Chem.*, 2008, **47**, 11269–11277, DOI: **10.1021/ic8018748**.
94 I. Dance, New insights into the reaction capabilities of His195 adjacent to the active site of nitrogenase, *J. Inorg. Biochem.*, 2017, **169**, 32–43, DOI: **10.1016/j.jinorgbio.2017.01.005**.
95 I. Dance, A pragmatic method for location of transition states and calculation of reaction paths., *Mol. Simul.*, 2008, **34**, 923–929.
96 I. Dance, A pragmatic method for location of transition states and calculation of reaction paths: erratum, *Mol. Simul.*, 2011, **37**, 257.
97 A. A. Gonzalez and C. D. Hoff, Entropy of binding molecular hydrogen and nitrogen in the complexes tricarbonylbis(tricyclohexylphosphine)transition metal (transition metal chromium, molybdenum, tungsten), *Inorg. Chem.*, 1989, **28**, 4295–4297, DOI: **10.1021/ic00322a023**.
98 D. L. M. Suess, C. Tsay and J. C. Peters, Dihydrogen Binding to Isostructural S = 1/2 and S = 0 Cobalt Complexes, *J. Am. Chem. Soc.*, 2012, **134**, 14158–14164, DOI: **10.1021/ja305248f**.
99 S. J. Irudayam and R. H. Henchman, Entropic Cost of Protein–Ligand Binding and Its Dependence on the Entropy in Solution, *J. Phys. Chem. B*, 2009, **113**, 5871–5884, DOI: **10.1021/jp809968p**.
100 R. J. Wilcock, R. Battino and E. Wilhelm, The solubility of gases in liquids 10. The solubility of He, Ne, Ar, Kr, N_2, O_2, CO, CO_2, CH_4, CF_4, and SF_6 in cyclooctane at 289 to 313 K, *J. Chem. Thermodyn.*, 1977, **9**, 111–115, DOI: **10.1016/0021-9614(77)90075-1**.
101 R. J. Wilcock, R. Battino, W. F. Danforth and E. Wilhelm, Solubilities of gases in liquids II. The solubilities of He, Ne, Ar, Kr, O_2, N_2, CO, CO_2, CH_4, CF_4, and SF_6 in n-octane 1-octanol, n-decane, and 1-decanol, *J. Chem. Thermodyn.*, 1978, **10**, 817–822, DOI: **10.1016/0021-9614(78)90154-4**.
102 R. J. Wilcock, J. L. McHale, R. Battino and E. Wilhelm, Solubility of gases in liquids. 12 Solubility of He, Ne, Ar, Kr, O_2, N_2, CO, CO_2, CH_4, CF_4, and SF_6 in octamethylcyclotetrasiloxane at 292 to 313 K, *Fluid Phase Equilib.*, 1978, **2**, 225–230, DOI: **10.1016/0378-3812(78)80011-9**.
103 R. Battino, T. R. Rettich and T. Tominaga, The Solubility of Nitrogen and Air in Liquids, *J. Phys. Chem. Ref. Data*, 1984, **13**, 563–600, DOI: **10.1063/1.555713**.
104 C. B. Kretschmer, J. Nowakowska and R. Wiebe, Solubility of Oxygen and Nitrogen in Organic Solvents from —25° to 50° C, *Ind. Eng. Chem.*, 1946, **38**, 506–509, DOI: **10.1021/ie50437a018**.
105 R. A. Warmack, B. B. Wenke, T. Spatzal and D. C. Rees, Anaerobic cryoEM protocols for air-sensitive nitrogenase proteins, *Nat. Protoc.*, 2024, **19**, 2026–2051, DOI: **10.1038/s41596-024-00973-5**.
106 C. N. Morrison, J. A. Hoy, L. Zhang, O. Einsle and D. C. Rees, Substrate Pathways in the Nitrogenase MoFe Protein by Experimental Identification of Small Molecule Binding Sites, *Biochemistry*, 2015, **54**, 2052–2060, DOI: **10.1021/bi501313k**.
107 T. Spatzal, K. A. Perez, J. B. Howard and D. C. Rees, Catalysis-dependent selenium incorporation and migration in the nitrogenase active site iron-molybdenum cofactor, *eLife*, 2015, **4**, e11620, DOI: **10.7554/eLife.11620**.
108 T. Spatzal, K. A. Perez, O. Einsle, J. B. Howard and D. C. Rees, Ligand binding to the FeMo-cofactor: Structures of CO-bound and reactivated nitrogenase, *Science*, 2014, **345**, 1620–1623, DOI: **10.1126/science.1256679**.
109 T. M. Buscagan, K. A. Perez, A. O. Maggiolo, D. C. Rees and T. Spatzal, Structural Characterization of Two CO Molecules Bound to the Nitrogenase Active Site, *Angew. Chem., Int. Ed.*, 2021, **60**, 5704–5707, DOI: **10.1002/anie.202015751**.
110 W. Kang, C. C. Lee, A. J. Jasniewski, M. W. Ribbe and Y. Hu, Structural evidence for a dynamic metallocofactor during N_2 reduction by Mo-nitrogenase, *Science*, 2020, **368**, 1381–1385, DOI: **10.1126/science.aaz6748**.
111 J. W. Peters, O. Einsle, D. R. Dean, S. DeBeer, B. M. Hoffman, P. L. Holland and L. C. Seefeldt, Comment on "Structural evidence for a dynamic metallocofactor during N_2 reduction by Mo-nitrogenase", *Science*, 2021, **371**, eabe5481, DOI: **10.1126/science.abe5481**.
112 W. Kang, C. C. Lee, A. J. Jasniewski, M. W. Ribbe and Y. Hu, Response to Comment on "Structural evidence for a dynamic metallocofactor during N_2 reduction by Mo-nitrogenase", *Science*, 2021, **371**, eabe5856, DOI: **10.1126/science.abe5856**.
113 C. C. Lee, W. Kang, A. J. Jasniewski, M. T. Stiebritz, K. Tanifuji, M. W. Ribbe and Y. Hu, Evidence of substrate binding and product release via belt-sulfur mobilization of the nitrogenase cofactor, *Nat. Catal.*, 2022, **5**, 443–454, DOI: **10.1038/s41929-022-00782-7**.